

# Binder Injection Additive Manufacturing

**Author names:** Hadley Brooks, Sam Chadwick, Alec Riding, Christian Saundry

**Affiliations:** University of Central Lancashire, Preston, PR12HE, United Kingdom

**Corresponding author:** Hadley Brooks, Hlbrooks1@uclan.ac.uk

## Abstract

This paper introduces binder injection additive manufacturing (AM), an emerging technology combining the advantages of material extrusion and binder jetting. Binder injection AM is demonstrated to be a versatile and capable manufacturing process. This paper details the basic theory underpinning binder injection AM, equipment modifications, nozzle-powder interactions, and process parameter investigations. A diverse array of powders and binders, including glass/PVA, cement/sodium silicate, sand/PVA, sawdust/pine resin, sawdust/epoxy, polystyrene/ABS slurry and sugar/sugar syrup were evaluated, with preliminary results indicating significant potential for the binder injection method in handling an expansive spectrum of powdered materials, especially low-cost and recycled powders. Print tests showcased the capability of this method to produce complex geometries quickly and accurately. The study presents the relationship between binder injection rates and printed track dimensions. Intersecting tool paths are explored and are found to be possible with this method. Post-processing methods for enhancing part strength are presented. Finally, recommendations for future work are provided.

## 1. Introduction:

This paper introduces a new AM process, binder injection. Binder injection is a hybrid of two AM processes, material extrusion and binder jetting, and works by injecting a binder into a powder vat to selectively consolidate regions of powder. Binder injection shares commonalities with related technologies such as direct writing, direct ink writing, dynamic mould deposition, rapid liquid printing, solid matrix assisted printing, injection 3D cement printing, injection 3D printing and liquid printed metal [1-8]. In a 2020 review paper Zhao and He used the term embedded 3D printing (EMB3D) to refer to this group of technologies [9]. EMB3D processes excel at printing a wide range of materials and allow for non-planar or freeform printing strategies. The supporting medium is often a gel but can also be other materials with low shear strength such as powders [3, 10]. To-date most EMB3D research has focussed on small-scale 3D printing of soft-materials for bioprinting or soft robotics applications, however large-scale prints with cement and liquid metals have also been demonstrated [11, 12]. Printing into a support

medium removes the need for support structures and allows liquids with slow curing or setting times to be deposited with minimal negative influences from gravity. The following sections introduce binder injection and details how it compares with a closely related technology binder jetting.

### 1.1 Binder injection AM

The main difference between other EMB3D processes and binder injection is that the primary build material and the support material are the same. A schematic of the binder injection process is shown in Figure 1, and a time lapse of the process can be seen in the supplementary materials.

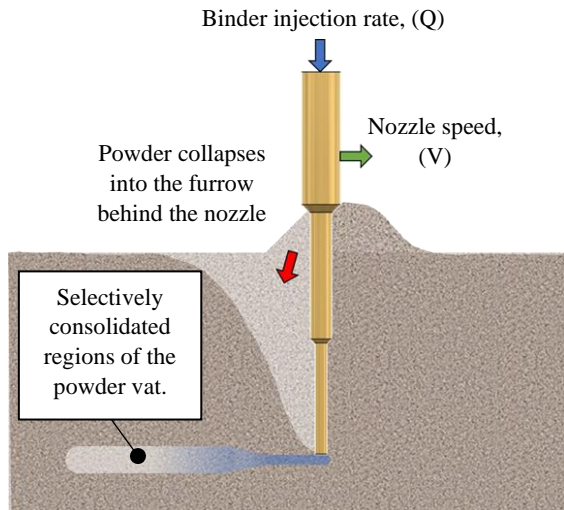


Figure 1. Schematic of the Binder Injection AM process.

Binder injection is a very versatile process due to the range of binding mechanisms that are possible. Table 1 summarises the main five binding mechanisms, however combinations of each mechanism and multi-binder interactions are also possible.

The interaction between the powder and the binder involves complex interconnected physical and chemical processes depending on the binder/powder combinations. The simplest case is where a displacing binder fully displaces the support medium, in which case the process would be identical to other EMB3D technologies. In this case the binder is the build material, and the size of the printed track is a function of the injection rate, nozzle speed and binder contraction/expansion.

For adhesive, reactive, dissolving, and thermal binders the relationship between the track size and the injection rate is more complicated. If the following assumptions are made; moderate binder viscosity, slow solidification times, and the surface tension overcomes gravity and capillary forces, then the binder can be assumed to fill the powder interstitial voids without displacing the powder in a region following the nozzle tip. In this instance a simple relationship between volumetric binder injection rate ( $Q$ ), nozzle velocity ( $V$ ) and powder packing density ratio ( $\rho$ ) can be used to determine the printed track cross-sectional area ( $X$ ). The ratio  $Q/V$  represents the injection rate  $E$  in volume per unit of nozzle travel.

$$X = E/\rho = Q/\rho V \quad \text{Equation 1.}$$

Where  $X$  = track cross-sectional area ( $\text{mm}^2$ ),  $E = Q/V$  ( $\text{mm}^3/\text{mm}$ ),  $\rho = \frac{\text{Solid volume}}{\text{Total volume}}$ ,  $Q$  = injection rate ( $\text{mm}^3/\text{s}$ ),  $V$  = nozzle speed ( $\text{mm}/\text{s}$ ).

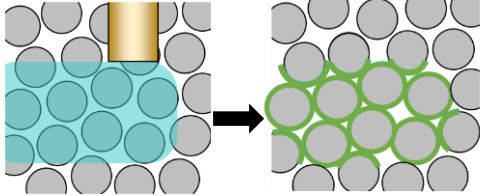
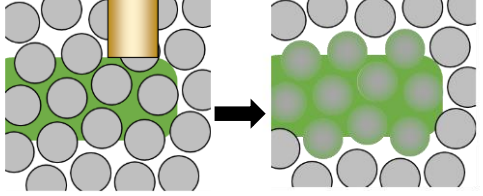
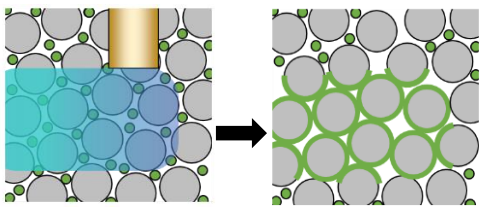
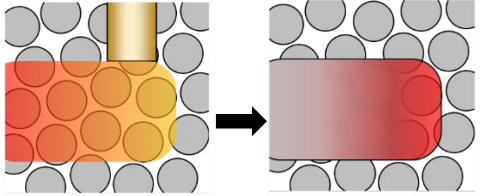
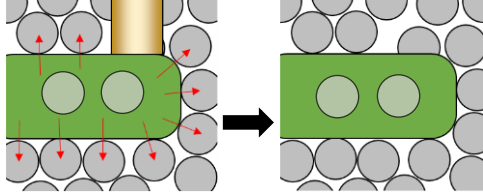
Equation 1 will not be accurate for binders that have too low viscosity and/or low surface tension as the liquid will tend to diffuse further into the powder creating a larger unsaturated track.

## 1.2 Binder injection vs binder jetting

Binder injection AM has some benefits over the related AM technology binder jetting, particularly for the use of low-cost materials and waste materials. Binder jetting requires the binder to be jetted onto the top layer of powder where it selectively consolidates a thin layer of material. Then a new layer of fine powder is spread on top. This process is repeated many times. Spreading the thin powder layers adds significant time to the build process and limits the type of powders that can be used to very fine powders ( $20 \mu\text{m}$  to  $100 \mu\text{m}$ ) with good flowability [13, 14]. Additionally, the binder must be jetted from a printhead onto the powder surface in small droplets, this constrains the liquid binders to a narrow range of viscosities, surface tensions and concentrations. Because there is no powder spreading step in binder injection, the process is very robust for a variety of powders. The powders can have a wide range of particle sizes and poor flowability, opening the opportunity for the processing of low-cost powdered materials.

The following sections will present preliminary investigations into binder injection AM.

Table 1. Binding mechanisms for binder injection additive manufacturing.

<p><b>Adhesive Binders:</b> A low viscosity binder is injected into the powder and fills the interstitial voids. The solvent evaporates leaving behind a network of bonded particles.</p> <p>Example: PVA glue injected into sand.</p>	
<p><b>Reactive Binders:</b> A chemical reaction forms a new interconnected material or the formation of a matrix.</p> <p>Example: Sodium silicate injected into cement.</p>	
<p><b>Dissolving Binders:</b> An injected solvent dissolves the powder (or a binder mixed with the powder) which is subsequently recast as a solid. A binder may also be dissolved in a solvent before injection.</p> <p>Example: ABS/Acetone slurry injected into ABS plastic granules.</p>	
<p><b>Thermal Binders:</b> A hot liquid is injected into the powder and solidifies as it cools. If the binder is sufficiently hot it could also melt the powder before cooling creating an alloy.</p> <p>Example: Liquid wax injected into wax powder.</p>	
<p><b>Displacing Binders:</b> A viscous liquid partially or fully displaces the powder then solidifies, creating a composite part.</p> <p>Example: Epoxy injected into chopped carbon fibres.</p>	

## 2. Methodology

### 2.1 Equipment

A Mini Kossel delta 3D printer from Think3dPrint3d was modified for binder injection, as shown in Figure 2. The delta architecture is useful as multiple motors are engaged when moving the nozzle through the powder, helping to overcome friction forces. The extruder motor was reconfigured to drive a syringe pump and the hotend was replaced with a stepped brass nozzle with a 3mm diameter outlet. A 200mm diameter vat was 3D printed to hold the powder. A silicone tube is used to convey binder from the syringe pump to the

nozzle. To simplify operation of the syringe pump the extruder motor steps/mm was adjusted in the firmware so 1mm of extrusion results in 1mm of syringe piston movement.

### 2.2 Materials

A range of powders with differing size, shape and solid fraction were selected to demonstrate the binder injection process. The powders were not modified except for a coarse sieve before loading into the vats. Image analysis software Fiji [15] was used to measure the particle sizes and the stationary funnel method was used to measure the angle of

repose [16]. The solid fraction of the powders were measured using the water displacement method.

A wide range of binders were also chosen allowing for testing of adhesive, reactive and dissolving binding mechanisms.

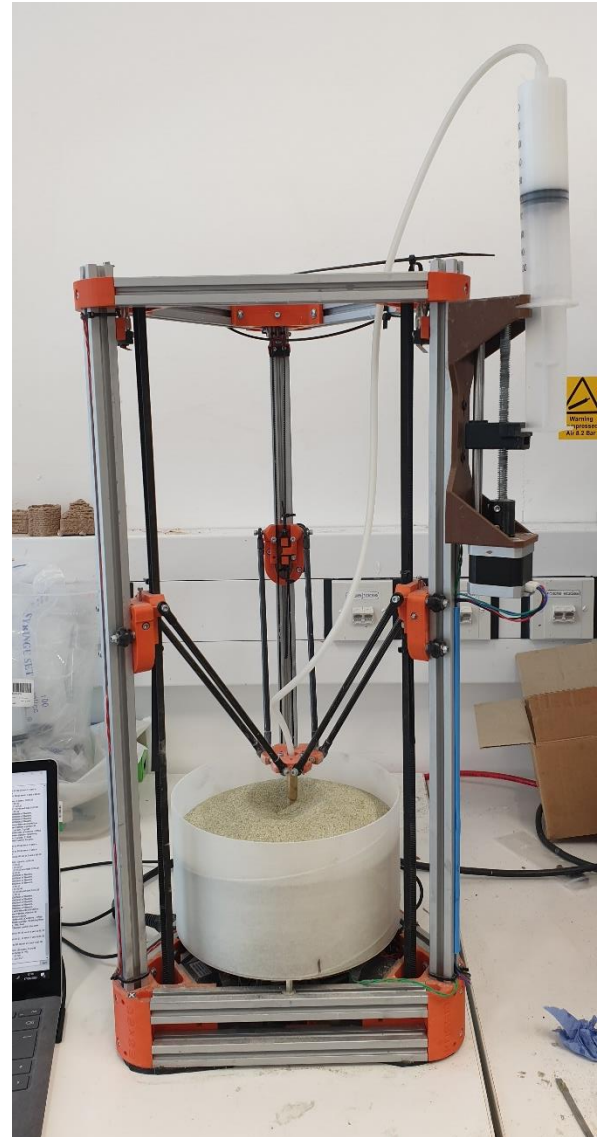


Figure 2. Modified delta 3D printer for binder injection AM.

Table 2. Powder properties.

Powder	Brand	Angle of repose (deg)	Mean particle size (mm)	Min - Max particle size (mm)	Powder solid fraction (%)
Sand	Dry Pavior Sand	34	0.66	0.34 – 1.7	71.0
Medium grit recycled glass	United Abrasives Ltd	34	0.58	0.21 - 1.3	73.5
Cement	Carlton Fence Post-Ecofix	41	0.046	0.013 – 1.7	74.0
Sawdust	NA	43	0.25	0.062 – 1.2	54.0
Granulated Sugar	Silver Spoon	-	0.46	-	-
Granulated polystyrene	Sourced from a variety of empty filament spools.	-	2.5	1.0 – 3.0	-

Table 3. Binder properties.

Binder	Brand	Notes
Polyvinylalcohol (PVA) glue	Scola Washable Glue	Mixed 3:1 with water to reduce viscosity.
Sodium silicate	Fisher Chemical 1.5 S.G.	Viscosity 20-400 mPa.s @ 20°C.
Sodium silicate	Chemiphase 40%	Viscosity 63-2,210 mPa.s @ 25°C.
Natural pine resin	NA	Dissolved to saturation in isopropanol.
Epoxy	Easy Composites EL2	Cured with slow hardener.
Granulated sugar	Silver Spoon	Dissolved to saturation in boiled water.

## 2.3 Print tests

### 2.3.1 Nozzle/powder interactions

To visualise the dynamics of the powder interacting with the nozzle, a rectangular vat was created with a transparent window on one side. The nozzle was moved at a speed of 10mm/s along the window inside a vat of sawdust and the movement of the particles was recorded by camera (see supplementary video).

### 2.3.2 Binder injection rate tests

To determine the relationship between track geometry and binder injection rate an array of 100mm tracks were printed at 4mm/s, varying the binder (PVA) injection rate  $E$  from 1.465 – 7.325 mm<sup>3</sup>/mm (Figure 3). The G-code was written

manually. A border was printed around the samples to aid material handling. The track widths were measured visually using Fiji software. Track heights were measured with manual calipers. Five height and width measurements were taken along each track and the mean measurement calculated.

### 2.3.3 Self-intersecting toolpaths

A diamond shaped toolpath was written to test what happens if the toolpath is self intersecting (Figure 4). Two self intersecting layers are stacked vertically to see if errors get compounded with successive layers. The PVA binder was injected at a rate of 8.79 mm<sup>3</sup>/mm into sand and glass powder.

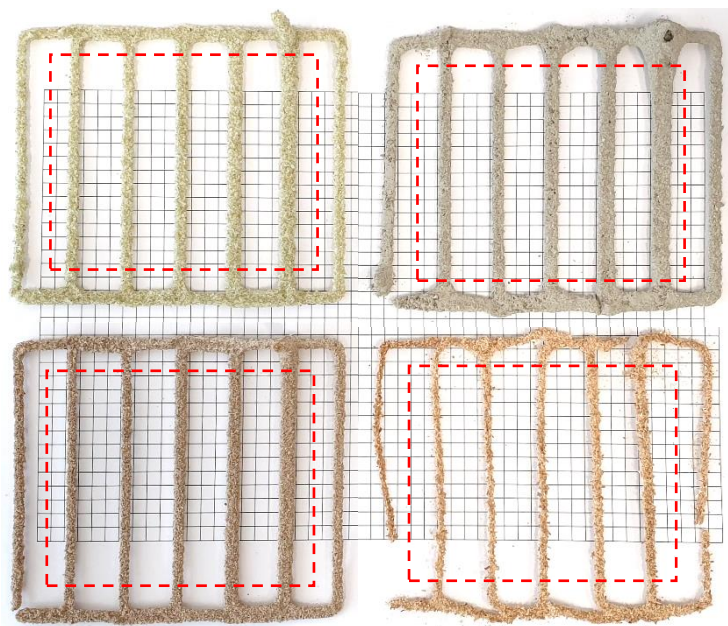


Figure 3. Tracks printed with PVA with varying binder injection rates. The outer frame is there to help support the sample tracks. The dashed red line indicates the area in which the height and width measurements were made.

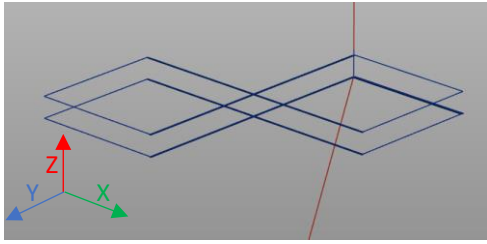


Figure 4. Self-intersecting tool path.

### 2.3.4 Case study prints

Four example parts (vase, moai, calibration cube and 3D Benchy), were printed with a variety of powder/binder combinations: glass/PVA, cement/sodium silicate, sand/PVA and sawdust/pine resin (Figure 5). All the binders utilise the adhesive binding mechanism except for cement/sodium silicate which uses the reactive binding mechanism. When sodium silicate and water is injected into cement the water will immediately begin to hydrate the cement particles forming calcium silicate hydrate (CSH) gel and other side products. The presence of sodium silicate will accelerate these hydration reactions [17].

*Slicer settings:* All parts were printed with 3 mm track widths and layer heights, single walls and a nozzle speed of 4mm/s. Ultimaker Cura was used to slice the models. The Z-Offset plugin from Cura Marketplace was used to adjust the height of the parts relative to the build plate to ensure the parts were positioned correctly within the powder vat. To print tracks with approximately 3mm height and width the flow setting was adjusted so that the extrusion rate in the G-code matches the corresponding extrusion rate from binder injection rate tests.

### 2.3.5 Post-processing

Depending on the powder/binder combination, the printed parts may benefit from post-print strengthening strategies. For example, water may be added to cement/sodium silicate samples to ensure complete curing. Glass/PVA samples may be heated in a furnace to burn out the PVA and sinter the glass particles. Sugar/sugar syrup samples can be coated/dipped in sugar syrup and freeze dried to reduce porosity and increase strength. The parts may also be infiltrated with wax or glue as is common for binder jetting parts. The following two methods were trialled here as proof of concept.



Figure 5. Left: CAD models for case study parts.

*Cement post-processing:* Two cement/sodium silicate (Chemiphase 40%) samples were printed, one left unchanged and one submerged in water until no bubbles emerged. The wetted sample was left to dry/cure. The compression tests were carried out 3 days after wetting.

*Glass post-processing:* Two glass/PVA specimens were printed, one left unchanged and one placed in a furnace (Thermo Scientific Lindberg/Blue M) in a graphite crucible and surrounded by plaster of Paris as a support medium. This prevents the glass from sagging. The furnace was heated up at a rate of 50°C per hour, to 300°C and left for three hours to burn away the PVA. The furnace was then heated up to 700°C at a rate of 100°C per hour and dwelled at that temperature for three hours to sinter the glass particles together into a solid object. The furnace was then allowed to cool to room temperature.

*Mechanical testing:* Cylindrical samples (nominally  $\varnothing 25\text{mm} \times 50\text{mm}$  high) were printed to be used for compression testing. The samples were printed with one wall and 3mm x3mm tracks. Printing just one wall reduces print time while capturing the internal powder which can be strengthened in the post-processing step. ASTM D695 standard was followed with a crosshead speed of 2mm/min. An Instron 68TM-5 universal testing machine was used for the tests.

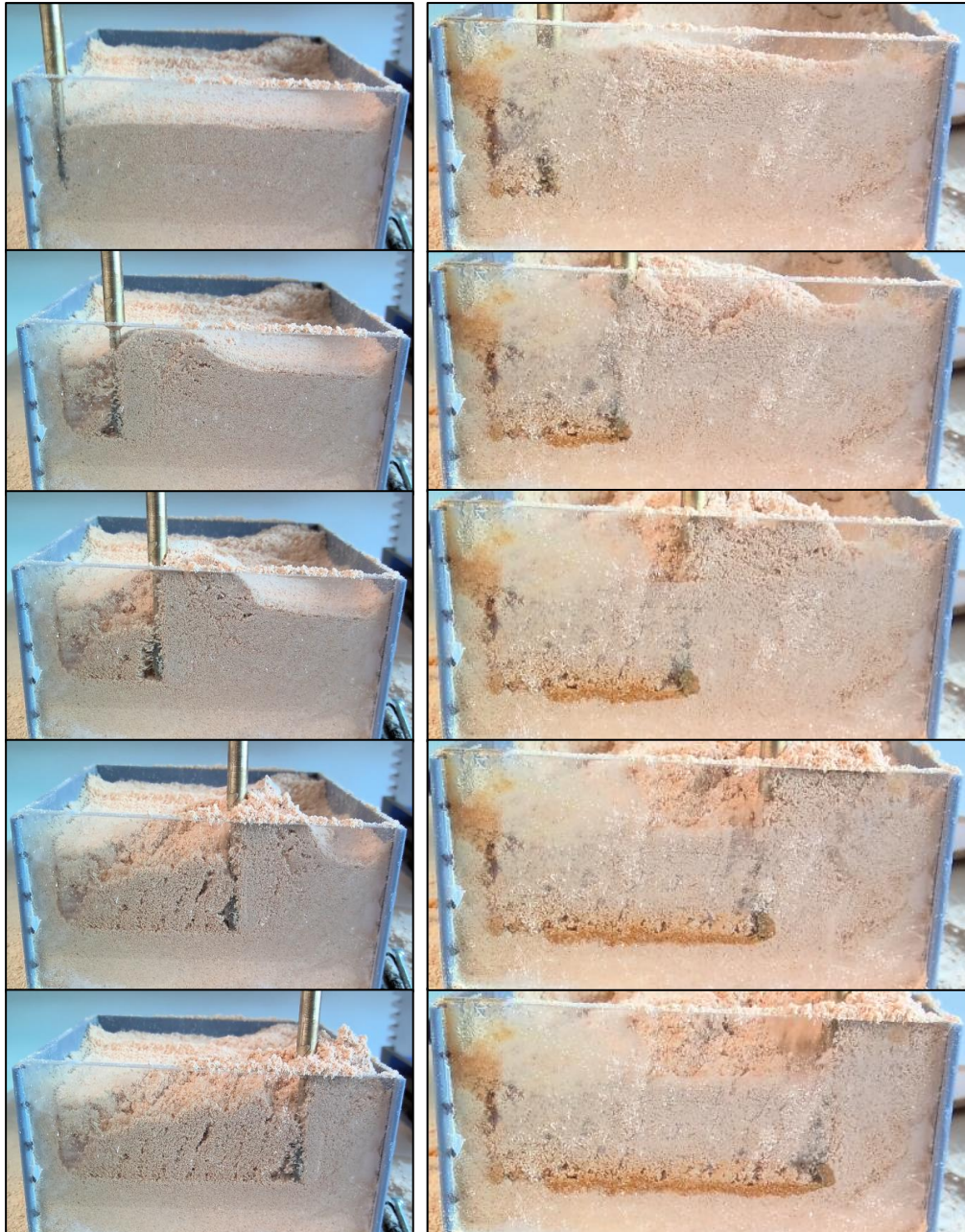


Figure 6. Left: Time lapse of the nozzle moving in a vat of sawdust without binder injection. Right: With pine-resin binder injection.

### 3. Results and discussion

#### 3.1 Nozzle/powder interactions

Moving the nozzle alongside a transparent wall provided visual information about how the nozzle and pine-resin binder interacted with the sawdust powder (Figure 6).

The powder around the nozzle can be split into four zones (Figure 7). Below the nozzle plane the powder is undisturbed. Attached to the front of the nozzle is a plow zone where the particles move with the nozzle. In front, and to the sides of the plow

zone is the shear zone where most of the resistance or drag on the nozzle comes from, due to the powder experiencing the highest levels of relative motion and shear. Behind the nozzle is the backfill zone. This backfilling behaviour is influenced by the properties of the powder and the speed of the nozzle. Compared to the smooth flow of sand and glass powders, the sawdust and cement exhibited stick-slip flow behaviour. Stick-slip flow is characterized by alternating periods of sticking (no motion) and slipping (sudden motion). The phenomenon is caused by the cohesive properties of the powder and inter-particle friction.

It should be noted that with this experimental setup the window is offset from the centreline of the nozzle path and prevents powder from flowing around the near side of the nozzle. This increased the size of the plow zone and slowed the rate of backfilling. It can be expected that during normal operation the backfilling would be slightly improved, and the size of the plow and shear zones reduced.

Visualising the flow of the powder helped to explain common defects found in the printed tracks. Powders with better flowability produced smoother more uniform printed tracks. It should be possible to improve powder flowability, and hence print quality, by drying the powders, or adding flow agents such as silicon dioxide, stearates, or talc. Other approaches could be to locally fluidise the powder around the nozzle by vibrating or rotating it

or by adding spider arms to the nozzle to agitate the surface powder. Printing too close to the surface of the powder can also reduce print quality as there is insufficient powder to ensure rapid backfilling. Experience showed the nozzle tip should always be 30mm below the 'global' surface level of the powder.

### 3.2 Binder injection rate

Track sizes increased with increasing injection rate, although this linear relationship only appears for injection rates over a threshold of  $2.93\text{mm}^3/\text{mm}$  (Figure 8). Below this threshold the track size seems to be constant. The nozzle outlet has inner and outer diameter of 3 and 4 mm respectively which seems to correlate with the minimum feature sizes. It is likely that reducing the nozzle diameter will reduce the minimum possible feature sizes.

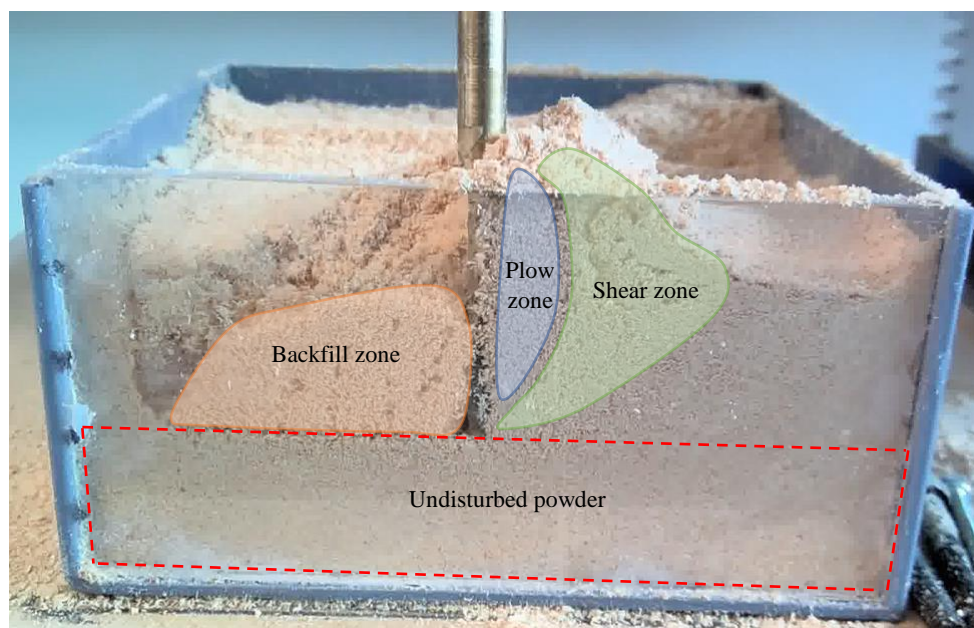


Figure 7. Nozzle moving in sawdust showing the backfill zone (orange), the plow zone (blue), the shear zone (green) and undisturbed powder (red dashes).



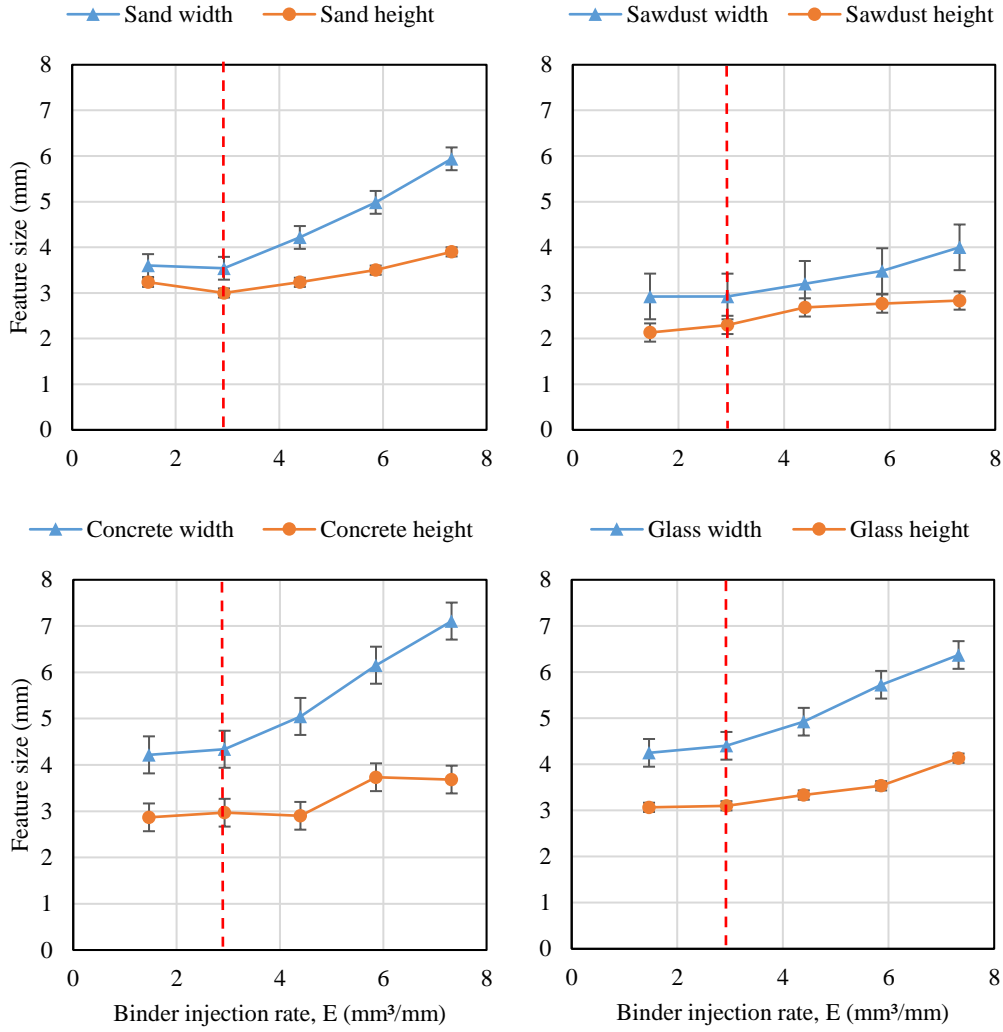


Figure 8. Track geometry vs binder injection rate. In all cases the track size increases linearly after a threshold of  $2.93\text{mm}^3/\text{mm}$  (red dashed line). Error bars show the average standard deviation for each material.

The slope of the linear relationship for the width of the tracks is greater than that of the heights, indicating the tracks become more elliptical at higher injection rates. At all binder injection rates, the track widths were greater than the track heights. This is likely due to nozzle/powder interactions. When the binder is diffusing through the powder immediately after injection there is an empty space in the backfill zone. Powder soon falls into the furrow, but this short delay is enough to stunt the upward flow front of the binder from the nozzle plane up into the backfill zone.

Figure 9 compares the cross-sectional area of the printed tracks against the predicted area using equation 1. The cross-sectional area was calculated by assuming an elliptical track and using mean width ( $W$ ) and height ( $H$ ) measurements, see equation 2.

$$X_{\text{Ellipse}} = \pi \left( \frac{W}{2} \times \frac{H}{2} \right) \quad \text{Equation 2.}$$

Above the binder injection rate threshold of  $2.93\text{mm}^3/\text{mm}$  the prediction is accurate with average absolute error between 2.2% (for sand) and 15.4% (for sawdust), suggesting the assumptions made in section 1.1 are valid for the PVA binder used in this experiment.

The highest print rate recorded for the PVA binder was  $83.2\text{mm}^3/\text{s}$ . This is considerably higher than rates achieved for desktop material extrusion printers in the range of  $3\text{--}10\text{mm}^3/\text{s}$  [18, 19] and on par with smaller binder jetting machines with a range of  $46.1\text{mm}^3/\text{s}$  to  $194\text{mm}^3/\text{s}$  [20]. Little effort was made to optimise print speed, so it is likely much higher print rates are possible. It would also be a trivial task to multiply the number of nozzles so that parallel printing of many parts is possible.

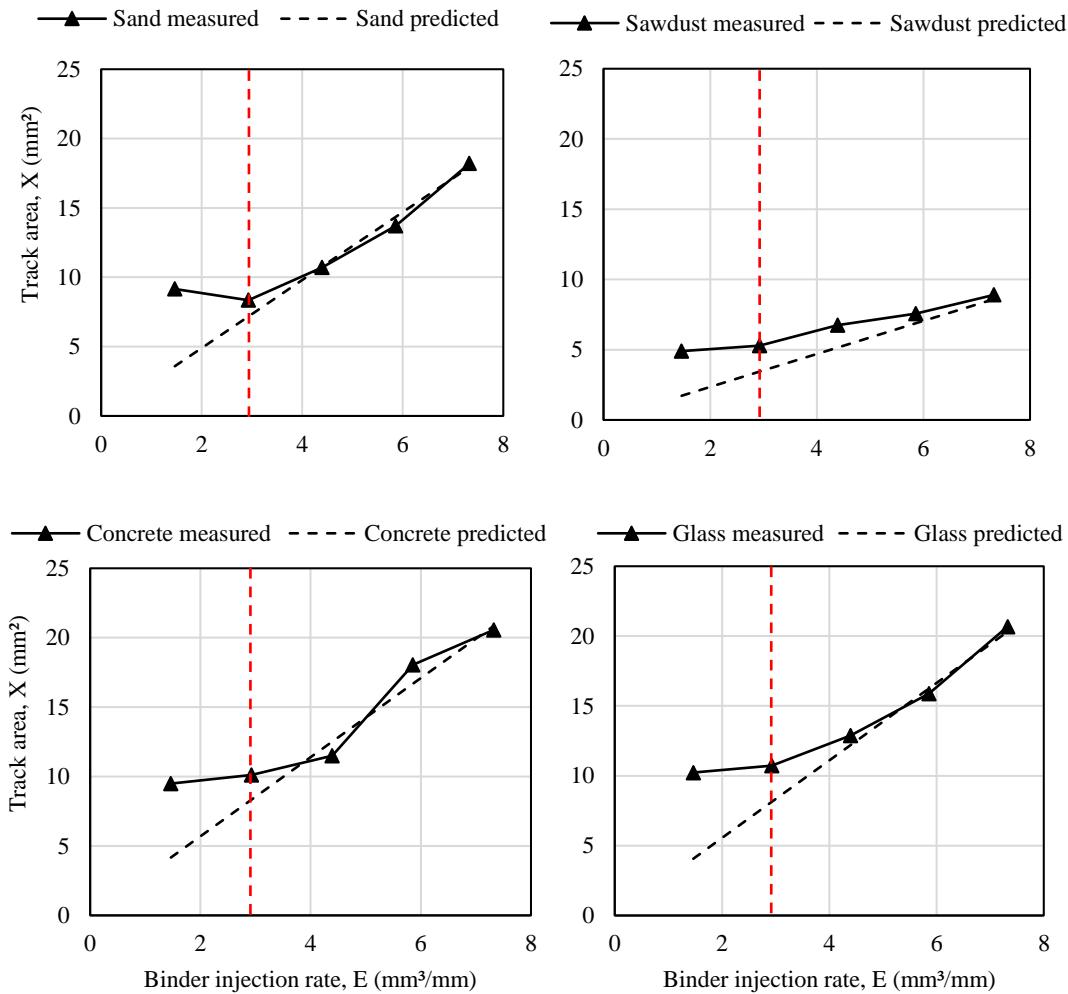


Figure 9. Measured track area vs predicted track area for a range of materials and PVA binder injection rates using Equation 1. The measured values converge to the predicted values after the  $E$  threshold of  $2.93 \text{ mm}^3/\text{mm}$ .

Two sodium silicate solutions with similar concentrations but different composition and viscosities (Fisher Chemical 1.5 S.G. and Chemiphase 40%) were injected into cement powder. The results in Figure 10 show that the track width is influenced by changes in binder properties. For these samples printed with higher binder injection rates, the relationship between injection rate and track width did not match well with equation 1. This highlights a weakness in the predictive capabilities of equation 1 as it does not consider the effects of capillary action or other mechanisms that can disperse the binder in powder to a greater extent.

Single printed tracks are often partially hollow once dry. This becomes more evident with larger tracks such as the samples shown in Figure 11. When printing more complex parts, with multiple layers and adjacent tracks, the size of the hollow area can

be reduced or eliminated entirely as subsequent passes of the nozzle disturbs the previous tracks collapsing the cavities.

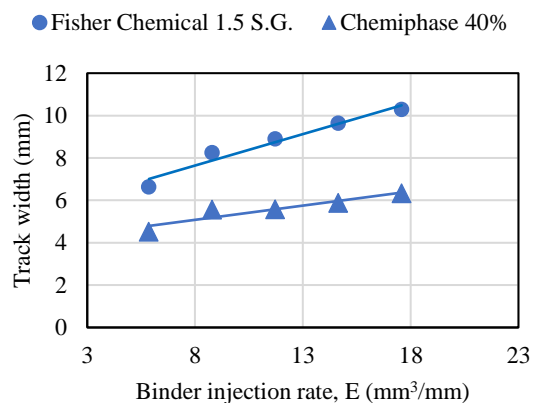


Figure 10. Comparison of different sodium silicate binders on the track width.



Figure 11. Hollow tubes were consistently formed in large single tracks bound with sodium silicate.

The cause of the cavities is not fully understood but is likely to be due to two main mechanisms. The first is powder displacement during injection. When a liquid is injected into a powder, it may displace the particles to some degree. The second mechanism is drying gradients, the drying process often proceeds from the outside to the inside, with the outer layer drying first and becoming rigid. As the interior continues to dry the reduction in volume due to shrinkage of the binder leads to the formation of a hollow cavity, especially if the outer shell does not allow for inward movement. Understanding how to control the size of the cavity may allow for control over the macroscopic density of the printed components.

### 3.3 Self-intersecting toolpaths

Parts printed with self-intersecting tool paths are shown in Figure 12. The intersection point seems largely unaffected by the nozzle returning to the same location. There is no evidence the nozzle distorted or disturbed the previously printed track. The cross over point is thicker than the rest of the part, but not double the volume as may be expected i.e., 14.2% thicker for the sand sample and 10.2% thicker for the glass sample. This shows the method to be forgiving to toolpath intersection and may allow toolpath strategies to be simplified without significant loss in component quality.

### 3.4 Case study prints

Knowledge of print parameters was used to print four example parts with different geometries and powder/binder combinations. The powder was found to sufficiently support the printed parts until the binder dried or cured. Drying times depended on the volume of the part and the permeability of the powder. For the parts shown in Figure 13 the drying times at room temperature was 1 to 4 days. These

can be greatly accelerated by placing the vats in a heated chamber or dehydrating atmosphere. The cement/sodium silicate moai cured in less than one day. One downside of binder injection is that you cannot know if a part is ready to be taken out of the powder vat until you try it.



Figure 12. Custom diamond toolpath designed to test self-intersection of the toolpath printed with sand/PVA and glass/PVA.

The sawdust/pine resin 3D Benchy was the most complex object as it required the printing of isolated islands and many non-printing travel moves. Due to oozing of the binder during travel moves, and the stick-slip flow of the sawdust, the 3D Benchy had the most defects, although the build did successfully complete.

The strength of the parts is sufficient for handling. The cement parts seemed to have the highest strength due to the reactive binding mechanisms.

Surface deviation analysis was carried out for the calibration cube to demonstrate printing accuracy for the sand/PVA combination (Figure 14). The results show most of the surface is within  $\pm 0.75$  mm of the CAD geometry. The main sources of error are due to rounding of corners in the horizontal plane, or due to artefacts from slicing with coarse 3x3 mm track sizes. The rounding of the corners is likely due to viscoelastic effects of the PVA binder as it was dragged around the corners. This defect is not seen on the top and bottom layers which contain more infill.

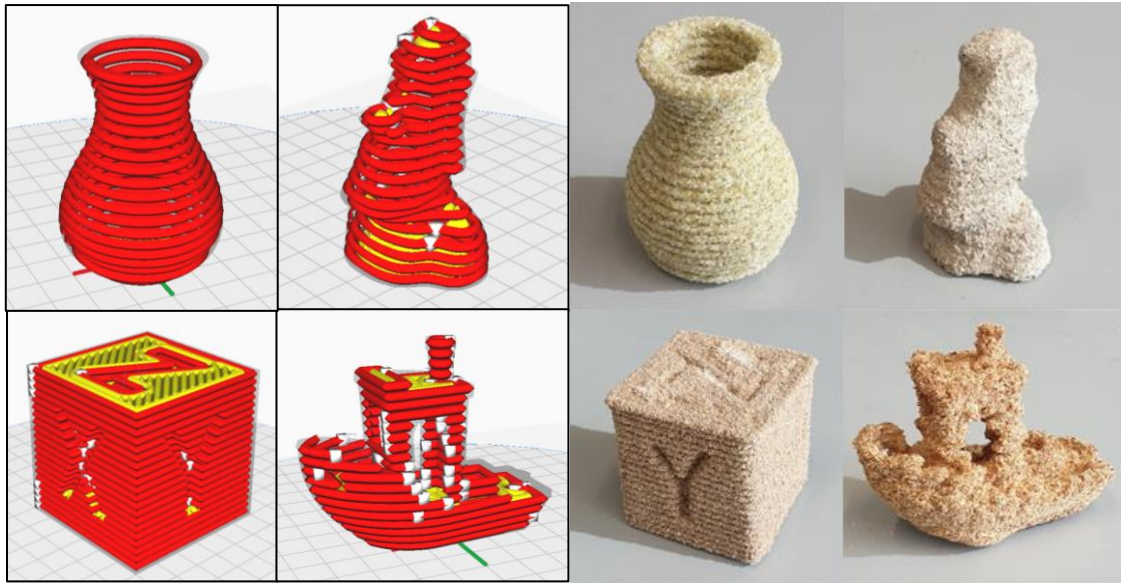


Figure 13. Example printed parts Left: Cura toolpath Previews. Right: Crushed glass/PVA vase, cement/sodium silicate moai, sand/PVA calibration cube and sawdust/pine resin 3D Benchy. For context, the printed parts are approximately 50-65mm high and print time was 20-30 minutes each.

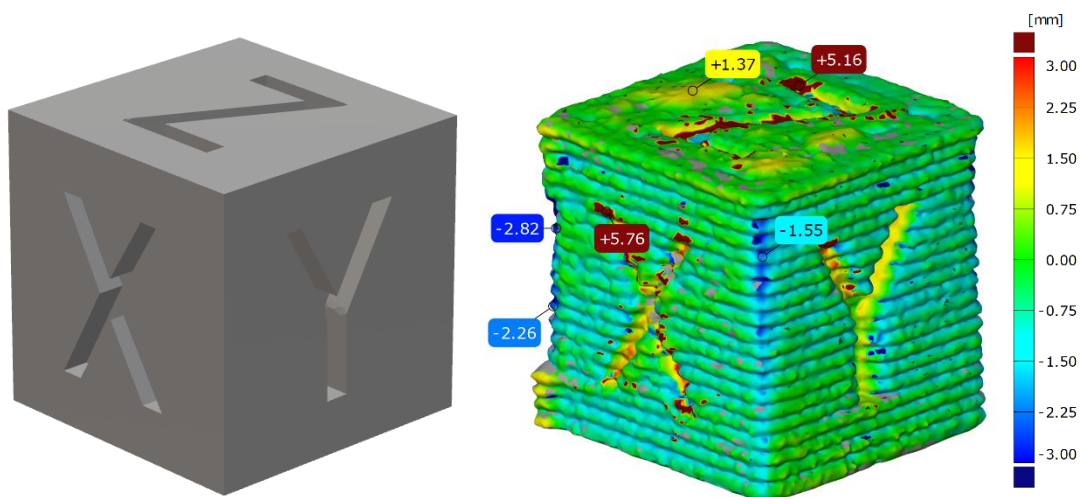


Figure 14. Surface deviation analysis comparing a cube printed with sand/PVA against the CAD model.

### 3.6 Additional material combinations

Additional material combinations were tested, although these were printed without prior optimisation of the binder injection rates. These material combinations include sugar/sugar syrup, sawdust/epoxy and granulated polystyrene waste/abs-acetone slurry and further demonstrate the versatility of the process to print a wide range of materials. Parts printed with these material combinations can be seen in Figure 15. The sugar/sugar syrup Moai and the polystyrene/abs

slurry are examples of dissolving binder mechanisms and can result in homogenous parts with high strengths. The cup made from irregular 2-3 mm polystyrene granules demonstrates the capability to print with extremely coarse granules.

### 3.7 Post-processing results

Significant increases in part strength were observed using the post-processing methods outlined in section 2.3.5.



Figure 15. Left: Sugar/Sugar syrup moai. Middle: Granulated polystyrene waste/ABS-acetone cup. Right: Sawdust/Epoxy cup.

**Cement samples:** Figure 16 shows a 252% increase in strength for the cement sample that went through a post curing step by saturating the part in water and allowing it to cure further. The strength increase to 1.3 MPa is considerably lower than the 3 to 10 MPa expected for fence post mix after 3 days. This suggests the sample was either not fully cured or lacked the density of conventional cement.

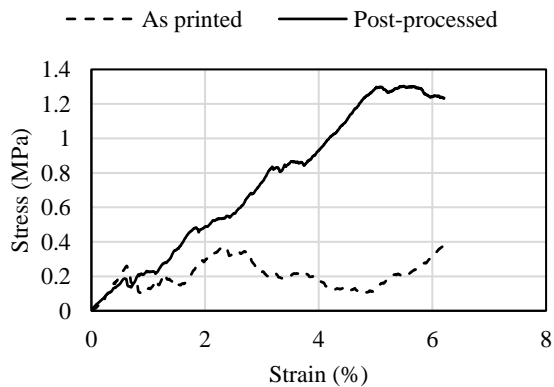


Figure 16. Compressive strength of as printed and post-cured cement/sodium silicate samples.

**Glass samples:** Sintering of the glass sample resulted in a volume decrease of 20% (Figure 17).



Figure 17. Glass samples. Left: As printed. Right: Reduced size after sintering.

Sintering increased the compressive strength by 1,345% to 12 MPa (Figure 18). While this is a good increase, the final strength is far below commonly quoted figures for bulk soda lime glass of 700-1000 MPa. This is not surprising as volume reductions of 40-60% are expected for full densification. Nevertheless, sintering shows promise as a strengthening process for a wide range of binder injection materials including glasses, ceramics, and metals.

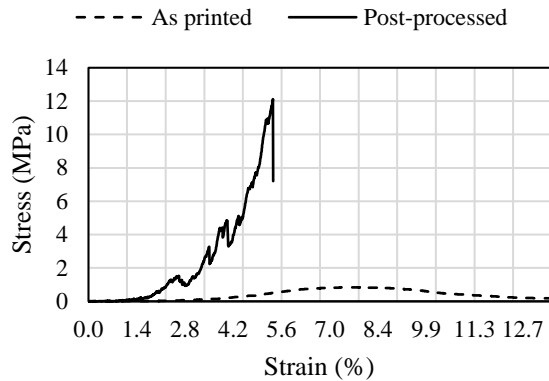


Figure 18. Compressive strength for sintered and un-sintered glass samples.

### 3.8 Binder injection applications

Binder injection is well-suited for applications requiring high build speed and the production of large parts that don't demand high resolutions. This makes it ideal for fabricating objects such as furniture and architectural features, including statues and gargoyles, where fine detail is less critical. One of its most significant advantages is its versatility in terms of materials; binder injection can work with almost any material, including local industrial waste powders like crushed glass, granulated polymers, or sawdust. Additionally, it can process low-cost, abundant materials such as sand, creating structures with a sandstone-like texture that are suitable for decorative or structural purposes.

For more demanding applications, binder injection can be used to print metal, glass, or ceramic parts, which can then be densified through a sintering step to improve their strength and mechanical properties. In this research, the resolution of the printed parts was primarily defined by the nozzle size. However, it is highly likely that higher resolution parts can be achieved using smaller nozzles, which could pave the way for applications in fields such as soft robotics and medical devices, where finer details and more complex geometries are required.

## 4. Conclusion

Binder injection AM, a novel process combining elements of material extrusion and binder jetting, has demonstrated significant potential. By leveraging the benefits of both techniques, binder injection allows for the use of a wide variety of

materials, particularly those that are low-cost or recycled materials. This work introduced five main binding mechanisms applicable to binder injection: adhesive, reactive, dissolving, thermal and displacing. Three mechanisms were demonstrated using different binder/powder combinations, providing a foundation for future explorations. The versatility of these mechanisms is key to the adaptability of binder injection across various materials.

An equation was developed to predict the cross-sectional area of printed tracks, and it showed reasonable accuracy across different materials and injection rates for adhesive binders. This predictive model serves as a useful tool for controlling and optimizing the geometry of printed components, especially when managing the interaction between binder injection rates and nozzle speed.

Nozzle-binder-powder interactions were studied to gain a deeper understanding of the process. Observations revealed key behaviours such as backfilling and powder displacement, which are critical to achieving consistent print quality. Toolpath strategies were also explored, particularly the behaviour of self-intersecting paths. It was found that intersecting toolpaths did not introduce significant print errors, which highlights the robustness of binder injection in handling complex toolpaths without compromising accuracy or introducing notable defects.

To showcase the versatility of the binder injection method, several case study parts were printed using different powder and binder combinations. Materials included glass, sand, sawdust, and cement, and the resulting parts demonstrated the flexibility of the process. Surface deviation analysis indicated that the overall print accuracy was within acceptable limits, given the size of the nozzle.

Finally, post-processing methods were trialed for glass and cement samples, leading to substantial improvements in mechanical strength. For instance, sintering of glass samples, and post-curing of cement samples provided a significant increase in compressive strength. These results show that post-processing is an effective option for enhancing the durability of printed parts and making them suitable for a wider range of applications.

## 5. Future work

Future work should focus on expanding the range of nozzle sizes for both small-scale and larger-scale printing applications. This includes evaluating the impact of various nozzle geometries on the printing process, particularly for complex freeform structures, which could benefit from the use of 6-axis robotic arms. Such an approach would also allow for testing novel freeform print paths that are not constrained by conventional Cartesian movements.

Another key area of research involves the nozzle angle during printing. Investigating the effect of angled or offset nozzles could yield insights into how these variations impact print quality, material deposition, and overall part strength. Additionally, integrating spider arms or similar mechanisms around the nozzle for powder agitation, or using vibrations for local powder fluidisation, could improve print precision and consistency.

Further investigation into multi-binder systems is also necessary. The ability to print with multiple binders could allow for the creation of multi-material parts with distinct regions offering different properties. This would open opportunities for more complex and functional component designs. Advancements in binder material science would support this goal by providing a broader range of binder-powder compatibility.

Finally, scaling up production through parallel printing with large nozzle arrays holds promise for increasing throughput and reducing the time required for large-scale manufacturing. Such developments, combined with multi-material capabilities, would make binder injection more competitive in industrial applications, especially where rapid production and multifunctionality are critical.

**Funding:** This research did not receive any specific grant from funding agencies in the public, commercial, or not-for-profit sectors.

## 5. References

1. Saadi, M.A.S.R., et al., *Direct Ink Writing: A 3D Printing Technology for Diverse Materials*. *Advanced Materials*, 2022. **34**(28): p. 2108855.
2. Gratson, G.M., M. Xu, and J.A. Lewis, *Direct writing of three-dimensional webs*. *Nature*, 2004. **428**(6981): p. 386-386.
3. Courtial, E.-J., A. Colly, and C. Marquette, *Dynamic Molding: Additive manufacturing in partially ordered system*. *Additive Manufacturing*, 2022. **51**: p. 102598.
4. Hack, N., et al., *Injection 3D Concrete Printing (I3DCP): Basic Principles and Case Studies*. *Materials*, 2020. **13**(5): p. 1093.
5. Hajash, K., et al., *Large-Scale Rapid Liquid Printing*. *3D Printing and Additive Manufacturing*, 2017. **4**(3): p. 123-132.
6. Tibbits, S.J., et al., *Liquid metal printing*. 2023, Google Patents.
7. Shin, S., H. Kwak, D. Shin, and J. Hyun, *Solid matrix-assisted printing for three-dimensional structuring of a viscoelastic medium surface*. *Nature Communications*, 2019. **10**(1): p. 4650.
8. Tabakova, V., C. Klug, and T.H. Schmitz, *Injection 3D Printing of Doubly Curved Ceramic Shells in Non-Synthetic Particle Suspensions*. *Materials*, 2024. **17**(16): p. 3955.
9. Zhao, J. and N. He, *A mini-review of embedded 3D printing: supporting media and strategies*. *Journal of Materials Chemistry B*, 2020. **8**(46): p. 10474-10486.
10. Grosskopf, A.K., et al., *Viscoplastic Matrix Materials for Embedded 3D Printing*. *ACS Applied Materials & Interfaces*, 2018. **10**(27): p. 23353-23361.
11. Lowke, D., et al., *Injection 3D concrete printing in a carrier liquid - Underlying physics and applications to lightweight space frame structures*. *Cement and Concrete Composites*, 2021. **124**: p. 104169.
12. Sparrman, B., S. Kernizan, J. Laucks, and S. Tibbits. *Liquid Printed Metal*. [Web page] 2022 19/07/2022]; Available from: <https://selfassemblylab.mit.edu/liquid-printed-metal>.
13. Ziaee, M. and N.B. Crane, *Binder jetting: A review of process, materials, and methods*. *Additive Manufacturing*, 2019. **28**: p. 781-801.
14. Miyanaji, H., *Binder jetting additive manufacturing process fundamentals and the resultant influences on part quality*. 2018.
15. Schindelin, J., et al., *Fiji: an open-source platform for biological-image analysis*. *Nature Methods*, 2012. **9**(7): p. 676-682.

16. Beakawi Al-Hashemi, H.M. and O.S. Baghabra Al-Amoudi, *A review on the angle of repose of granular materials*. Powder Technology, 2018. **330**: p. 397-417.
17. Wang, Z., Y. Sun, S. Zhang, and Y. Wang, *Effect of sodium silicate on Portland cement/calcium aluminat cement/gypsum rich-water system: strength and microstructure*. RSC Advances, 2019. **9**(18): p. 9993-10003.
18. Go, J. and A.J. Hart, *Fast Desktop-Scale Extrusion Additive Manufacturing*. Additive Manufacturing, 2017. **18**: p. 276-284.
19. Badarinath, R. and V. Prabhu, *Real-Time Sensing of Output Polymer Flow Temperature and Volumetric Flowrate in Fused Filament Fabrication Process*. Materials, 2022. **15**(2): p. 618.
20. Mitchell, S., *Improving Properties of Binder jet Printed Parts Using Hierarchical Binders*. 2022, The University of Liverpool (United Kingdom): England. p. 286.